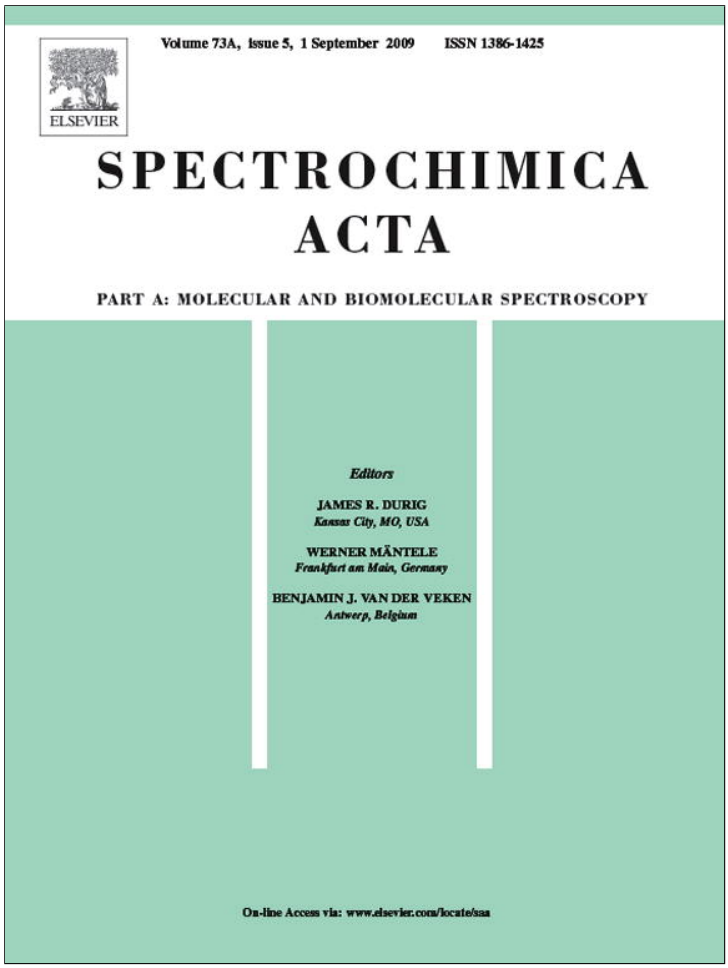

Spectrochimica Acta Part A 73 (2009) 833–840

Contents lists available at ScienceDirect

Spectrochimica Acta Part A: Molecular and Biomolecular Spectroscopy

journal homepage: www.elsevier.com/locate/saa

Spectroscopic study of molecular structures of novel Schiff base derived from o-phthaldehyde and 2-aminophenol and its coordination compounds together with their biological activity

Sayed M. Abdallah [a], Gehad G. Mohamed [b,*], M.A. Zayed [b], Mohsen S. Abou El-Ela [c]

[a] Works University, Aswan, Egypt
[b] Botany Department, Faculty of Science, Cairo University, 12613, Giza, Egypt
[c] Chemistry Department, Faculty of Science, Cairo University, 12613, Giza, Egypt

ARTICLE INFO

Article history:
Received 27 November 2008
Received in revised form 18 March 2009
Accepted 14 April 2009

Keywords:
Schiff base
Transition metal complexes
IR
^{1}H NMR
ESR
Solid reflectance
Magnetic moment
Molar conductance
Thermal analysis
Biological activity

ABSTRACT

New Schiff base (H_2L) ligand is prepared via condensation of o-phthaldehyde and 2-aminophenol. The metal complexes of Cr(III), Mn(II), Fe(II), Fe(III), Co(II), Ni(II), Cu(II) and Zn(II) with the ligand are prepared in good yield from the reaction of the ligand with the corresponding metal salts. They are characterized based on elemental analyses, IR, solid reflectance, magnetic moment, electron spin resonance (ESR), molar conductance, ^{1}H NMR and thermal analysis (TGA). From the elemental analyses data, the complexes are proposed to have the general formulae $[M(L)(H_2O)n]\cdot yH_2O$ (where M = Mn(II) ($n = 0, y = 1$), Fe(II) ($n = y = 0$), Co(II) ($n = 2, y = 0$), Ni(II) ($n = y = 2$), Cu(II) ($n = 0, y = 2$) and Zn(II) ($n = y = 0$), and $[MCl(L)(H_2O)]\cdot yH_2O$ (where M = Cr(III) and Fe(III), $y = 1$–2). The molar conductance data reveal that all the metal chelates are non-electrolytes. IR spectra show that H_2L is coordinated to the metal ions in a bi-negatively tetradentate manner with ONNO donor sites of the azomethine N and deprotonated phenolic-OH. This is supported by the ^{1}H NMR and ESR data. From the magnetic and solid reflectance spectra, it is found that the geometrical structures of these complexes are octahedral (Cr(III), Fe(III), Co(II) and Ni(II) complexes), tetrahedral (Mn(II), Fe(II) and Zn(II) complexes) and square planar (Cu(II) complex). The thermal behaviour of these chelates is studied and the activation thermodynamic parameters, such as, E^*, ΔH^*, ΔS^* and ΔG^* are calculated from the DrTGA curves using Coats-Redfern method. The parent Schiff base and its eight metal complexes are assayed against two fungal and two bacterial species. With respect to antifungal activity, the parent Schiff base and four metal complexes inhibited the growth of the tested fungi at different rates. Ni(II) complex is the most inhibitory metal complex, followed by Cr(III) complex, parent Schiff base then Co(II) complex. With regard to bacteria, only two of the tested metal complexes (Mn(II) and Fe(II)) weakly inhibit the growth of the two tested bacteria.

1. Introduction

Schiff bases have been used extensively as ligands in the field of coordination chemistry, some of the reasons are that the intramolecular hydrogen bonds between the (O) and the (N) atoms which play an important role in the formation of metal complexes and that Schiff base compounds show photochromism and thermochromism in the solid state by proton transfer from the hydroxyl (O) to the imine (N) atoms [1]. A large number of Schiff bases and their complexes have been investigated for their interesting and important properties, such as their ability to reversibly bind oxygen, catalytic activity in the hydrogenation of olefins, photochromic properties and complexing ability towards some toxic metals, furthermore complexes of Schiff bases showed promising applications in biological activity and biological modeling applications [2–4].

Schiff bases are important class of compounds in medicinal and pharmaceutical field. They show biological applications including antibacterial [5,6], antifungal [7] and antitumor activity [8]. Microbes encounter a variety of metal ions in the environment and interact with them, which is sometimes beneficial or detrimental depending on the chemical/physical nature and oxidation state of the metal ion. Of particular interest are those metal ions, which exist mostly as cations (or cationic complexes), oxyanions, as salts or oxides in crystalline form or as amorphous precipitates in insoluble form. The microbes have the ability to bind to metal ions present in the external environment at the cell surface and to transport them into the cell for various intracellular functions [9]. The incidence of life-threatening Aspergillus infections has risen in recent years [10]. Although Aspergillus fumigatus accounts for the majority of cases

* Corresponding author.
E-mail address: ggenidy@hotmail.com (G.G. Mohamed).

1386-1425/$ – see front matter © 2009 Elsevier B.V. All rights reserved.
doi:10.1016/j.saa.2009.04.005

of human aspergillosis, the number of infections caused by other Aspergillus species has increased [11]. The emerging threat posed by these species is especially important to understand because of their inherent reduced susceptibility to many antifungal agents [12]. Few reports describe Aspergillus species as a possible cause of sternal wound infection [13].

As an extension of our work on the structural characterization of Schiff base ligands and their metal complexes [14–17], the main target of the present article is to study the coordination behaviour of H_2L Schiff base that incorporate several binding sites towards Cr(III), Mn(II), Fe(III), Fe(II), Co(II), Ni(II), Cu(II) and Zn(II) ions, also to evaluate the relative thermal stability of the synthesized complexes and to examine their antimicrobial activity against different species of bacteria and fungi.

2. Experimental

2.1. Materials and reagents

All chemicals used were of the analytical reagent grade (AR), and of highest purity available. They included o-phthaldehyde (Sigma); 2-aminophenol (Sigma); Cu(II) chloride dihydrate (Prolabo); Co(II) and Ni(II) chlorides hexahydrates (BDH); ferrous chloride dihydrate (Sigma), Zn(II) chloride dihydrate (Ubichem), Cr(III) chloride hexahydrate (Sigma); Mn(II) chloride and Fe(III) chloride hexahydrate (Prolabo). Zinc oxide and EDTA (Analar), ammonia solution (33% v/v) and ammonium chloride were supplied from El-Nasr pharm. Chem. Co., Egypt. Organic solvents used included absolute ethyl alcohol, diethylether, and dimethylformamide (DMF). These solvents were spectroscopic pure from BDH. Hydrogen peroxide, hydrochloric and nitric acids (MERCK) were used. De-ionized water collected from all glass equipments was usually used in all preparations.

Two *Aspergillus* species: *A. flavus* Link and *A. niger* V. Tiegh and two Bacteria: *Escherichia coli* and *Staphyllococcus aureus* were used for this study. All isolates were from Microanalytical Center, Faculty of Science, Cairo University.

2.2. Instruments

The molar conductance of solid complexes in DMF was measured using Sybron-Barnstead conductometer (Meter-PM.6, $E = 3406$). Elemental microanalyses of the separated solid chelates for C, H and N were performed in the Microanalytical Center, Cairo University. The analyses were repeated twice to check the accuracy of the data. Infrared spectra were recorded on a PerkinElmer FT-IR type 1650 spectrophotometer in wave number region 4000–400 cm^{-1}. The spectra were recorded as KBr pellets. The ^1H NMR spectra were recorded with a JEOL EX-270 MHz in d_6-DMSO as solvent, where the chemical shifts were determined relative to the solvent peaks. The solid ESR spectra of the complexes were recorded with ELEXSYS E500 Bruker spectrometer in 3 mm pyrex tubes at 298 K. Diphenylpicrydrazide (DPPH) was used as a g-marker for the calibration of the spectra. The solid reflectance spectra were measured on a Shimadzu 3101pc spectrophotometer. The molar magnetic susceptibility was measured on powdered samples using the Faraday method. The diamagnetic corrections were made by Pascal's constant and $Hg[Co(SCN)_4]$ was used as a calibrant. The thermogravimetric analysis (TGA and DrTGA) was carried out in dynamic nitrogen atmosphere (20 mL min^{-1}) with a heating rate of 10 °C min^{-1} using Shimadzu TGA-50H thermal analyzer. The mass spectra were recorded by the EI technique at 70 eV using MS-5988 GC–MS Hewlett-Packard instrument in the Microanalytical Center, Cairo University.

2.3. Synthesis of Schiff base (H_2L)

Hot solution (60 °C) of 2-aminophenol (2.18 g, 20 mmol) was mixed with hot solution (60 °C) of o-phthaldehyde (1.34 g, 10 mmol) in 50 mL ethanol. The resulting mixture was left under reflux for 4 h and the solvent was evaporated till deep yellow oil product is separated. This oil is poured on ice cold HCl whereupon the yellow crystalline product is separated. The formed solid product was separated by filtration, purified by crystallization from ethanol, washed with diethyl ether and dried under vacuum. The yellow product is produced in 80% yield.

2.4. Synthesis of metal complexes

The metal complexes were prepared by adding equimolar amounts of hot solution (60 °C) of the appropriate metal chloride (1 mmol) in an ethanol–water mixture (1:1, 25 mL) to the hot solution (60 °C) of the Schiff base (0.316 g, 1 mmol) in the same solvent (25 mL). The resulting mixture was stirred under reflux for 1 h whereupon the complexes precipitated. The resulting precipitates were filtered off, washed several times with a 1:1 ethanol:water mixture and diethyl ether and dried under vacuum. The analytical data for C, H and N were repeated twice.

2.5. Biological activity

2.5.1. Disc diffusion assay for Aspergillus spp.

The *in vitro* activity of H_2L and its metal complexes was tested against two *Aspergillus* spp. (*Aspergillus flavus* and *Aspergillus niger*). The test organisms were identified to the species level by standard methods [18] and maintained at −70 °C on Sabouraud dextrose agar slant until tested. This assay employed an investigational method that used the reference RPMI 1640 agar supplemented with 2% glucose as the test medium [19]. Ten μg/ml of the tested compounds were prepared by using blank paper disks (6.3 mm in diameter), the disks were allowed to dry at room temperature prior to their use in disk diffusion assays. The inoculum density to be used in the test was adjusted spectrophotometrically to 10^6 CFU/ml. The previously prepared Schiff base and its metal complexes disks were then placed on the inoculated plates, and the plates were incubated at 35 °C. The results were examined after 5 days of incubation and the % of inhibition zone was compared to that of control.

2.5.2. Disc diffusion assay for bacteria

Disk diffusion testing was by standard NCCLS methods [20] using Mueller–Hinton plates supplemented with sheep blood and inoculated with 0.5 McFarland standard. Disks with 10 μg of the tested compounds were applied. After overnight incubation at 35 °C, the inhibition zone diameters were measured.

2.5.3. Determination of MIC

Antimicrobial activities of the compounds were estimated by a minimum inhibitory concentration (MIC, μg/ml) in the usual fashion [21].The evaluation of the inhibitory effect of the Schiff base and their complexes on the microbial growth was carried out by the twofold serial dilution method. Mueller–Hinton broth and Sabouraud liquid medium were employed as culture media for bacteria and fungi, respectively. The compounds were dissolved in dimethylsulfoxide (DMSO). Test inoculums of 5×10^4 M bacteria ml^{-1} and 10^3 M spores ml^{-1} were applied. The absence of microbial growth after an incubation period of 24 h at 37 °C for bacteria or of 5 days at 30 °C for fungi was taken to be a criterion of effectiveness. In every case, MIC was determined. The MIC was defined as the lowest drug concentration that inhibits growth by 50%. The amount of DMSO in the medium was 1% and did not affect the growth of the microorganisms tested. There were three replicates

for each dilution. Results were always verified in three separate experiments.

3. Results and discussion

3.1. Schiff base characterization

The Schiff base, H_2L, is subjected to elemental analyses. The results of elemental analyses (C, H and N) with molecular formula and the melting point are presented in Table 1. The results obtained are in good agreement with those calculated for the suggested formula and the melting point is sharp indicating the purity of the prepared Schiff base. The structure of the Schiff base under study is given below in Fig. 1.

The structure of this Schiff base is also confirmed by IR and ^1H NMR spectra, which will be discussed in detailed manner together with its metal complexes later. It takes the following IUPAC name: 2-((1))-2-{2-[(1)-2-aza-2-2-(2-hydroxyphenyl)vinyl]phenyl}-1-azavinyl)phenol.

3.2. Composition and structure of Schiff base complexes

The isolated solid complexes of Cr(III), Mn(II), Fe(II), Fe(III), Co(II), Ni(II), Cu(II) and Zn(II) ions with the Schiff base H_2L ligand were subjected to elemental analyses (C, H, N and metal content), IR, magnetic studies, ESR, ^1H NMR, molar conductance and thermal analysis (TGA), to identify their tentative formulae in a trial to elucidate their molecular structures. The elemental analyses confirm that the complexes have 1:1 molar ratio between the metal ions and the ligand. The results of elemental analyses listed in Table 1 suggest the proposed general formulae of the prepared complexes as: $[MCl(L)(H_2O)]\cdot yH_2O$ (M = Cr(III), Fe(III); y = 1–2), $[M(L)(H_2O)_2]\cdot yH_2O$ (M = Co(II), Ni(II); y = 0–2) and $[M(L)]\cdot yH_2O$ (M = Mn(II), Fe(II), Cu(II), Zn(II); y = 0–2). The complexes are found to be insoluble in common organic solvents such as ethanol, methanol, acetone, 1,4-dioxane, water and chloroform but soluble in DMF and DMSO.

3.3. Molar conductivity measurements

The molar conductivities of 10^{-3} M solutions of the dissolved chelates in DMF are measured at 25 °C and listed in Table 1. The molar conductance values are found to be 9.21–14.55 Ω^{-1} mol^{-1} cm^2 indicating that, these chelates are non-electrolytes.

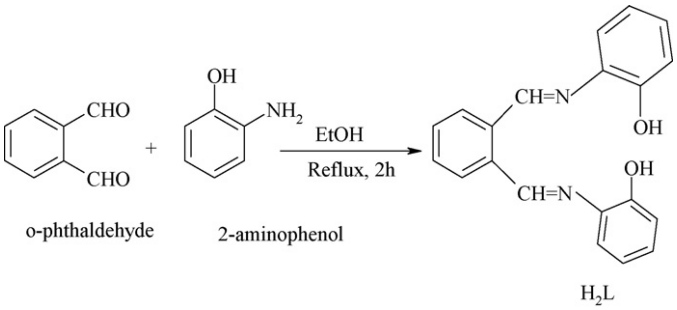

Fig. 1. Preparation of H_2L ligand.

3.4. IR spectra and mode of bonding

The IR data of the spectra of H_2L Schiff base and its complexes are listed in Table 2. Upon comparison it was found that the azomethine υ(C=N) stretching vibration is found in the free ligand at 1642 cm^{-1}. This band is shifted to 1654–1657 cm^{-1} in the complexes indicating the participation of the azomethine nitrogen in coordination (M–N) [15]. The υ(OH), υ(C–O) and δ(OH) vibrations are observed at 3068, 1243 and 1456 cm^{-1} for H_2L. The existence of water of hydration and/or water of coordination in the spectra of the complexes render it difficult to get conclusion from the υ(OH) group of the H_2L ligand, which will be overlapped by those of the water molecules. The participation of the OH group is further confirmed by clarifying the effect of chelation on the υ(C–O) and in-plane bending, δ(OH) vibrations. The participation of the phenolic O atom in the complex formation was proved by the shift in position of these bands to 1239–1246 and 1450–1452 cm^{-1} [22]. New bands are found in the spectra of the complexes in the regions 468–530, which are assigned to υ(M–O) stretching vibrations. The bands at 417–472 have been assigned to υ(M–N) mode.

Therefore, the above arguments together with the elemental analyses indicated that H_2L ligand behaves as a dibasic tetradentate ligand coordinated to the metal ions via the azomethine N and deprotonated phenolic O.

3.5. ^1H NMR spectra

The chemical shifts of the different types of protons in the ^1H NMR spectra of the H_2L ligand and its diamagnetic Zn(II) complex are listed in Table 3. Upon examinations it is found that the phe-

Table 1
Analytical and Physical data of H_2L ligand and its metal complexes.

Compound	m.p. (°C)	Colour (% yield)	% Found (calcd.)				$\mu_{eff.}$ (B.M.)	Λ_m Ω^{-1} mol^{-1} cm^2
			C	H	N	M		
H_2L	100	Yellow	68.09	4.41	6.94	–	–	–
($C_{20}H_{16}N_2O_2$)		(80)	(67.97)	(4.01)	(6.60)			
$[CrCl(L)(H_2O)]\cdot H_2O$	>300	Brown	54.87	3.79	6.58	11.99		
$C_{20}H_{18}ClCrN_2O_4$		(69)	(54.61)	(4.10)	(6.37)	(12.29)	4.15	10.96
$[Mn(L)]\cdot H_2O$	>300	Brown	61.77	4.22	7.45	14.05		
$C_{20}H_{16}MnN_2O_3$		(68)	(62.18)	(4.15)	(7.25)	(13.99)	4.69	14.55
[Fe(L)]	>300	Yellowish brown	64.90	3.39	7.98	15.08		
$C_{20}H_{14}FeN_2O_2$		(63)	(64.87)	(3.78)	(7.57)	(15.14)	4.89	9.21
$[FeCl(L)(H_2O)]\cdot 2H_2O$	>300	Yellowish brown	51.97	4.56	6.19	12.48		
$C_{20}H_{20}ClFeN_2O_5$		(63)	(52.23)	(4.35)	(6.09)	(12.19)	5.69	11.33
$[Co(L)(H_2O)_2]$	>300	Reddish brown	58.86	4.80	7.00	14.62		
$C_{20}H_{18}CoN_2O_4$		(59)	(58.68)	(4.40)	(6.85)	(14.43)	5.72	11.75
$[Ni(L)(H_2O)_2]\cdot 2H_2O$	>300	Brown	53.60	4.72	6.41	13.56		
$C_{20}H_{22}NiN_2O_6$		(66)	(53.90)	(4.94)	(6.29)	(13.26)	3.44	12.45
$[Cu(L)]\cdot 2H_2O$	>300	Green	57.77	4.22	6.76	15.23		
$C_{20}H_{18}CuN_2O_4$		(60)	(58.04)	(4.35)	(6.77)	(15.36)	1.98	14.16
[Zn(L)]	>300	Brown	63.52	3.36	7.55	17.07		
$C_{20}H_{14}N_2O_2Zn$		(58)	(63.32)	(3.69)	(7.39)	(17.15)	Diam.	13.11

Table 2
IR spectra (4000-400 cm^{-1}) of the H_2L ligand and its metal complexes.

Compound	ν(OH)	ν(C–O)	δ(OH)	ν(CH=N)	ν(M–O)	ν(M–N)
H_2L	3068br	1243m	1456m	1642sh	–	–
$[CrCl(L)(H_2O)]\cdot H_2O$	3179br	1240m	1452m	1656sh	530s	460w
$[Mn(L)]\cdot H_2O$	3176br	1240m	1452m	1655sh	545s	472s
[Fe(L)]	3139br	1240m	1451m	1655sh	478s	430w
$[FeCl(L)(H_2O)]\cdot 2H_2O$	3152br	1239m	1451sh	1654sh	472s	430w
$[Co(L)(H_2O)_2]$	3142br	1246m	1453m	1657sh	471m	421s
$[Ni(L)(H_2O)_2]\cdot 2H_2O$	3140br	1240m	1451m	1655sh	468m	417w
$[Cu(L)]\cdot 2H_2O$	3139br	1246m	1450m	1657sh	515w	472s
[Zn(L)]	3199br	1240m	1451m	1655sh	472s	421s

sh = sharp, m = medium, s = small, w = weak, br = broad.

nolic OH signal is found at 9.80 ppm in the spectrum of H_2L ligand. This signal is disappeared in case of [Zn(L)] complex indicating the participation of the phenolic OH group in chelation with proton displacement.

3.6. Magnetic susceptibility and electronic spectra measurements

The diffused reflectance spectrum of the Cr(III) chelate shows three absorption bands at 18,975 (ν_1), 27,240 (ν_2), and 28,860 cm^{-1} (ν_3) which are assigned to the three spin allowed transitions in the electronic spectrum, ν_1:$^4A_{2g} \rightarrow {}^4T_{2g}$, ν_2:$^4A_{2g} \rightarrow {}^4T_{2g}$ (F), and ν_3:$^4A_{2g} \rightarrow {}^4T_{1g}$ (P) [23]. The electronic spectrum of this Cr(III) chelate is in reasonable agreement with those reported in the literature [23]. The magnetic moment of this chelate measured at room temperature is 4.15 B.M., and corresponds to the expected value for octahedral Cr(III) complexes [23]. The diffused reflectance spectrum of the Mn(II) complex shows three bands at 16,645, 22,765 and 27,765 cm^{-1} assignable to $^6A_{1g} \rightarrow {}^4T_{1g}$, $^6A_{1g} \rightarrow {}^4T_{2g}$ (G) and $^6A_1 \rightarrow {}^4T_{2g}$ (D) transitions, respectively [23]. The magnetic moment value is 4.69 B.M., which indicates the presence of Mn(II) complex in tetrahedral structure.

From the diffused reflectance spectrum, it is observed that, the Fe(III) chelate exhibit a band at 20,750 cm^{-1}, which may be assigned to the $^6A_{1g} \rightarrow T_{2g}$ (G) transition in octahedral geometry of the Fe(III) complexes [24]. The $^6A_{1g} \rightarrow {}^5T_1g$ transition appears to be split into two bands at 17,876 and 14,980 cm^{-1}. The observed magnetic moment of Fe(III) complex is 5.69 B.M. Thus, the complexes formed have the octahedral geometry [23]. The spectrum shows also a band at 28,331 cm^{-1} which may attribute to ligand to metal charge transfer. The electronic spectrum of the Fe(II) complex displays two absorption bands at 16,540 and 18,670 cm^{-1} that are assigned to $^5E_g \rightarrow {}^5T_{2g}$ (D) transition [17]. In addition, the band at 24,495 cm^{-1} is assigned to L → M charge transfer. The observed magnetic moment of 4.89 B.M. is assigned to tetrahedral geometry [17].

The electronic spectrum of the Co(II) complex gives three bands at 16,666, 18,785 and 22,330 cm^{-1}. The bands observed are assigned to the transitions $^4T_{1g}$ (F) → $^4T_{2g}$ (F) (ν_1), $^4T_{1g}$ (F) → $^4A_{2g}$ (F) (ν_2) and $^4T_{1g}$ (F) → $^4T_{2g}$ (P) (ν_3), respectively, suggesting that there is an octahedral geometry around Co(II) ion [23,22]. The magnetic susceptibility value of 5.72 B.M. indicates an octahedral geometry [23,22]. The band at 24,680 cm^{-1} refers to the charge transfer occurring in this complex.

Table 3
^1H NMR data of H_2L and its Zn(II) complexes.

Compound	δ (ppm)	Assignments
H_2L	9.80	(br, 2H, Phenolic OH)
	8.089	(s, 2H, –CH=N)
	6.386–7.779	(m, 12H, ArH)
[Zn(L)]	8.12	(s, 2H, –CH=N)
	6.42–7.775	(m, 12H, ArH)

Table 4
ESR parameters for H_2L metal complexes.

Complex	$g_{\|\|}$	$g_\perp$	$^a g_{iso/av}$	$^b G$
$[Mn(L)]\cdot H_2O$	4.751	2.296	3.114	9.294
[Fe(L)]	2.346	4.765	3.959	0.125
$[FeCl(L)(H_2O)]\cdot 2H_2O$	2.202	3.295	2.931	0.156
$[Cu(L)]\cdot 2H_2O$	2.44	2.261	2.321	1.686

$^a 3g_{iso} = (g_\perp + g_{||} + 2)$.
$^b G = (g_{||} - 2)/(g_\perp - 2)$.

The Ni(II) complex reported herein has a room temperature magnetic moment value of 3.44 B.M.; which is in the normal range observed for octahedral Ni(II) complexes [23]. This indicates that, the complexes of Ni(II) are six coordinate and probably octahedral [23]. The electronic spectrum displays three bands, in the solid reflectance spectrum at ν_1:15,700 cm^{-1}:$^3A_{2g} \rightarrow {}^3T_{2g}$; ν_2:17,655 cm^{-1}:$^3A_{2g} \rightarrow {}^3T_{1g}$ (F) and ν_3:21,202 cm^{-1}:$^3A_{2g} \rightarrow {}^3T_{1g}$ (P). The spectrum shows also a band at 23,870 cm^{-1} which may be attributed to ligand-metal charge transfer. The μ_{eff} = 1.98 B.M. of the Cu(II) complex indicates the square planar geometry. The confirmation of this structure is obtained by the appearance of a band at 14,875 cm^{-1} and two shoulders at 18,962 and 12,085 cm^{-1}. These are assigned to $^2B_{1g} \rightarrow {}^2A_{1g}$, $^2B_{1g} \rightarrow {}^2B_{2g}$ and $^2B_{1g} \rightarrow {}^2E_{2g}$ transitions, respectively [23]. A moderately intense peak observed at 24,895 cm^{-1} is due to ligand-metal charge transfer.

The Zn(II) complex is diamagnetic and according to the empirical formula, it is proposed to have a tetrahedral geometry.

3.7. Electron spin resonance spectra (ESR)

The ESR data are listed in Table 4. The ESR spectra of the Cu(II) complex at room temperature exhibits anisotropic signals with g value $g_{||}$ = 2.44 and $g_\perp$ = 2.261 (Fig. 2 and Table 4) which is characteristic for axial symmetry [25]. Since the $g_{||}$ and $g_\perp$ values are closer to 2 and $g_{||} > g_\perp$ suggesting a tetragonal distortion around Cu(II) ion corresponding to elongation along the fourfold symmetry Z-axis [26]. The trend $g_{||} > g_\perp > g_e$ (2.0023) shows that the unpaired electron in localized in the d_{x2-y2} orbital of the Cu(II) ion in complexes [27]. In addition, exchange coupling interaction between two Cu(II) ions is explained by Hathaway expression $G = (g_{||} - 2)/(g_\perp - 2)$. When the value $G < 4.0$, a considerable exchange coupling is present in solid complex (G = 1.686) [25]. Kivelson and Neiman showed that for an ionic environment $g_{||}$ is normally 2.3 or larger, but for covalent environment $g_{||}$ are less than 2.3. The $g_{||}$ value for the Cu(II) complex is 2.44, consequently the environment is essentially ionic.

The ESR spectra of the solid Co(II), Ni(II) and Zn(II) complexes at room temperature do not show ESR signal because the rapid spin lattice relaxation of the Co(II), Ni(II) and Zn(II) (Fig. 3) broadness

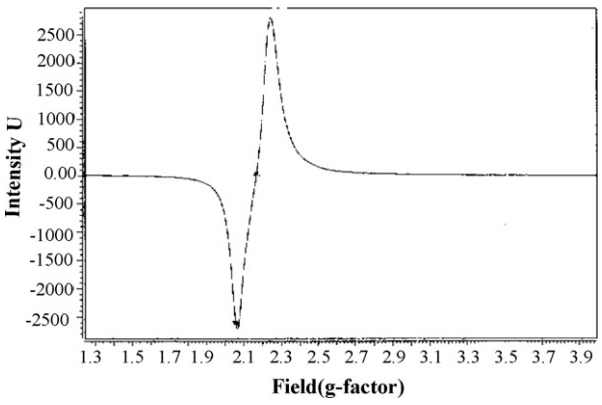

Fig. 2. ESR of Cu(II)-H_2L complex.

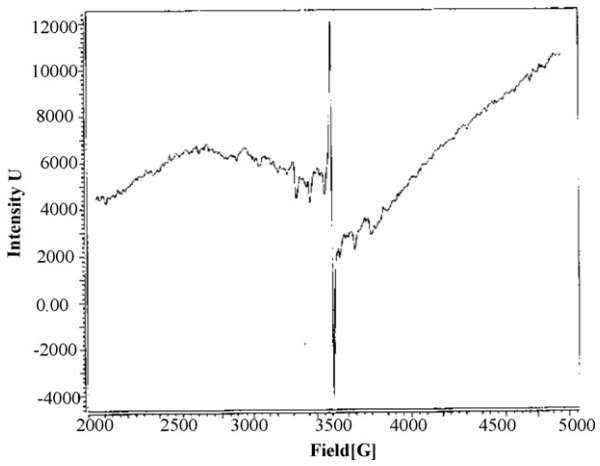

Fig. 3. ESR of Zn(II)-H_2L complex.

the lines at higher temperatures [25]. The ESR spectra only show signals that may be accounted for the presence of free radicals that can resulted from the cleavage of any double bond and distribution of the charge on the two neighbor atoms.

The ESR spectrum of the Mn(II) complex (Table 3) at room temperature give two signals with $g_{||} = 4.751$ and $g_{\perp} = 2.296$. This finding indicates that the complex is tetrahedral which is in agreement with the data of solid reflectance and magnetic moment measurements [25]. The ESR spectrum of the $[FeCl(L)(H_2O)]\cdot 2H_2O$ complex showed two signals observed at g values 2.202 and 3.295. These values can be respected as the signal of high spin state of the Fe(III) ($S = 5/2$) [25].

3.8. Thermal analyses (TGA and DrTGA)

The thermal analysis data are listed in Table 5 and the calculated thermodynamic parameters from DrTGA are listed in Table 6.

The thermograms of $[MCl(L)(H_2O)_3]\cdot xH_2O$ chelates (M = Cr(III) ($x = 1$) and Fe(III) ($x = 2$)) show four decomposition steps within the temperature range 30–1000 °C. The first step of decomposition within the temperature ranges 30–120 and 30–250 °C corresponds to the loss of hydrated and coordinated water molecules with a mass loss of 4.65% (calcd. 4.10%) and 11.51% (calcd. 11.75%) for Cr(III) and Fe(III) complexes, respectively. The energy of activation values were 43.65 and 52.15 kJ mol^{-1} for Cr(III) and Fe(III) complexes, respectively. The subsequent weight loss steps (120–1000 or 250–1000 °C) correspond to the removal of HCl, coordinated H_2O and the organic part of the ligand leaving metal oxide as a residue. The overall weight losses are found to be 83.35% (calcd. 82.71%) and 82.52% (calcd. 82.59%) for Cr(III) and Fe(III) complexes, respectively.

The TGA curves of the Co(II) and Ni(II)-chelates show three to four stages of decomposition within the temperature ranges of 30–1000 and 30–900 °C, respectively. For Ni(II) complex, the first stage at 30–130 °C corresponds to the loss of water molecules of hydration. The value of energy of activation for this dehydration step was found to be = 49.75 kJ mol^{-1}. While the subsequent stages involved the loss of coordinated H_2O and ligand molecules with a mass loss of 81.91% (calcd. 81.66%) and 75.71% (calcd. 75.06%) for Co(II) and Ni(II) complexes, respectively. The overall weight loss amounts to 81.91% (calcd. 81.66%) and 84.17% (calcd. 83.15%) for Co(II) and Ni(II) chelates, respectively.

On the other hand, [M(L)] (M = Fe(II) and Zn(II)) chelates exhibit three decomposition steps within the temperature range 70–1000 °C (mass loss = 79.99%; calcd. 80.54%) and 120–1000 °C (mass loss = 78.95%; calcd. 78.63%) which may accounted for the thermal decomposition of H_2L molecule in three steps in each complex leaving metal oxides as a residue for Fe(II) and Zn(II) complexes, respectively. The energies of activation for these six steps (three in each complex) were found to be = 60.55, 117.6 and 176.9 and 60.88, 82.99 and 162.5 kJ mol^{-1} for Fe(II) and Zn(II) complexes, respectively.

Each of $[Mn(L)]\cdot H_2O$ and $[Cu(L)]\cdot 2H_2O$ complexes were thermally decomposed in four steps within the temperature range from 40 to 1000 and 30 to 700 °C, respectively. The first decomposition step with an estimated mass loss of 4.95% (calcd. 4.66%) and 8.85% (calcd. 8.71%) occurred within the temperature range from 40 to 110 and 30 to 130 °C for Mn(II) and Cu(II) complexes, respectively. This step may be attributed to the liberation of the hydrated water molecules. The activation energy values for these losses were = 30.46 and 53.65 kJ mol^{-1} for Mn(II) and Cu(II) complexes, respectively. The remaining three decomposition steps of each complex were observed within the temperature ranges from 110 to 1000 and 140 to 700 °C for Mn(II) and Cu(II) complexes, respectively. The estimated mass losses of 77.06% (calcd. 77.20%) and 73.08% (calcd. 72.07%) are reasonably accounted for the removal of H_2L ligand in three steps for each complex as gases, for Mn(II) and Cu(II) complexes, respectively. The activation energies for these six losses were 78.64, 169.8 and 233.4 and 95.99, 147.6 and201.5 kJ mol^{-1} for the second, third and fourth steps, respectively.

3.9. Kinetic data

The thermodynamic activation parameters of decomposition processes of dehydrated complexes namely activation energy (E^*), enthalpy (ΔH^*), entropy (ΔS^*) and Gibbs free energy change of the decomposition (ΔG^*) were evaluated graphically by employing the Coats-Redfern relation [28]. The entropy of activation (ΔS^*), enthalpy of activation (ΔH^*) and the free energy change of activation (ΔG^*) were calculated and the data are summarized in Table 6.

Table 5
Thermal analyses (TGA) results of H_2L and its chelates.

Complex	Temp. range (°C)	$n^{\#}$	Mass loss total mass loss % found (calcd)	Assignment	Metallic residue
$[CrCl(L)(H_2O)]$	30–120	1.0	4.65 (4.10)	Loss of H_2O.	
H_2O	120–1000	3.0	78.70 (78.61) 83.35 (82.71)	Loss of HCl, H_2O and L	$1/2Cr_2O_3$
$[Mn(L)]\cdot H_2O$	40–110	1.0	4.95 (4.66)	Loss of H_2O.	
	110–1000	3.0	77.06 (77.20) 82.01 (81.86)	Loss of L.	MnO
[Fe(L)]	70–1000	3.0	79.99 (80.54)	Loss of L.	FeO
$[FeCl(L)(H_2O)]$	30–250	1.0	11.51 (11.75)	Loss of $3H_2O$.	$1/2Fe_2O_3$
$2H_2O$	250–1000	3.0	71.01 (70.84) 82.52 (82.59)	Loss of HCl and L.	
$[Co(L)(H_2O)_2]$	100–1000	3.0	81.91 (81.66)	Loss of $2H_2O$ and L	CoO
$[Ni(L)(H_2O)_2]$	30–130	1.0	8.46 (8.09)	Loss of $2H_2O$.	
$2H_2O$	130–900	3.0	75.71 (75.06) 84.17 (83.15)	Loss of $2H_2O$ and L.	NiO
$[Cu(L)]\cdot 2H_2O$	30–150	1.0	8.85 (8.71)	Loss of $2H_2O$.	
	150–700	3.0	73.08 (72.07) 81.93 (80.78)	Loss of L.	CuO
[Zn(L)]	120–1000	3.0	78.95 (78.63)	Loss of L.	ZnO

$n^{\#}$ = number of decomposition steps.

Table 6
The calculated thermodynamic parameters for the thermal decomposition data of H_2L metal complexes.

Complex	TG range (°C)	E^* (kJ mol^{-1})	A (S^{-1})	ΔS^* (JK^{-1} mol^{-1})	ΔH^* (kJ mol^{-1})	ΔG^* (kJ mol^{-1})
[CrCl(L)(H_2O)]	30–120	43.65	4.32×10^7	−44.63	54.35	77.43
H_2O	120–380	92.86	2.95×10^{11}	−82.67	127.2	156.2
	380–670	192.5	5.42×10^8	−126.3	145.4	189.3
	670–1000	115.7	3.66×10^9	−174.2	197.4	235.6
[Mn(L)]·H_2O	40–110	30.46	4.07×10^6	−34.99	42.88	54.56
	110–300	78.64	6.59×10^{10}	−95.83	109.7	138.7
	300–650	169.8	6.09×10^{11}	−152.4	162.5	182.7
	650–1000	233.4	5.23×10^8	−166.8	201.1	243.3
[Fe(L)]	70–320	60.55	3.18×10^9	−49.84	73.62	86.26
	320–700	117.6	4.50×10^{10}	−80.95	145.2	187.1
	700–1000	176.9	6.75×10^7	−143.7	186.7	223.6
[FeCl(L)(H_2O)]	30–250	52.15	5.16×10^8	−60.38	66.42	73.39
2H_2O	250–520	105.9	4.08×10^9	−108.3	126.3	139.3
	520–730	182.4	6.56×10^{11}	−157.6	192.4	203.9
	730–1000	256.3	7.56×10^7	−196.2	260.5	269.8
[Co(L)(H_2O)$_2$]	100–240	63.95	3.09×10^{10}	−53.46	72.76	96.86
	240–640	95.19	7.92×10^7	−109.2	147.6	175.7
	640–1000	127.9	4.69×10^{13}	−152.9	198.9	230.4
[Ni(L)(H_2O)$_2$]	30–130	49.75	3.13×10^7	−50.33	77.72	95.53
2H_2O	130–320	75.97	4.17×10^{10}	−89.77	133.2	140.2
	320–750	147.2	3.75×10^{12}	−140.3	186.7	222.4
	750–900	199.2	6.97×10^8	−176.5	250.1	260.5
[Cu(L)]·2H_2O	30–150	53.65	1.43×10^{13}	−33.66	48.97	69.86
	150–330	95.99	6.37×10^{11}	−90.97	116.2	138.86
	330–520	147.6	4.22×10^6	−142.3	176.4	189.7
	520–700	201.5	7.32×10^{84}	−172.3	205.3	250.3
[Zn(L)]	120–330	60.88	7.85×10^9	−40.75	59.66	73.36
	330–640	82.99	4.99×10^8	−80.08	109.7	121.99
	640–1000	162.5	5.96×10^{10}	−136.6	158.8	192.4

The activation energies of decomposition were found to be in the range 22.95–243.4 kJ mol^{-1}. The high values of the activation energies reflect the thermal stability of the complexes. The entropy of activation was found to have negative values in all the complexes, which indicates that the decomposition reactions proceed with a lower rate than the normal ones.

3.10. Structural interpretation

The structures of the complexes of Schiff base with Cr(III), Mn(II), Fe(III), Fe(II), Co(II), Ni(II), Cu(II) and Zn(II) ions were confirmed by the elemental analyses, IR, molar conductance, magnetic, solid reflectance and thermal analysis data. Therefore, from the IR spectra, it is concluded that H_2L behaves as a bi-negatively tetradentate ligand coordinated to the metal ions via the azomethine N and deprotonated phenolic-O. From the molar conductance data, it is found that the complexes are non-electrolytes. On the basis of the above observations and from the magnetic and solid reflectance measurements, octahedral, terahderal and square planar geometries are suggested for the investigated complexes. As a general conclusion, the investigated Schiff base behaves as a tetradentate and its metal complexes structurs can be given as shown below (Fig. 4).

3.11. Biological activity

In testing the antimicrobial activity of these compounds, we used more than one test organism to increase the chance of detecting antibiotic principles in the tested materials. The sensitivity of a microorganism to antibiotics and other antimicrobial agents was determined by the assay plates. Metal complexes: Mn(II), Fe(II), Fe(III), Cu(II) and Zn(II) virtually lack any noticeable antifungal activities. A detectable antifungal activity was observed in case of using H_2L, Cr(III), Co(II) and Ni(II) at concentrations above 50 μg ml^{-1}.

With regard to *A. flavus*, Table 7 shows that the parent Schiff base and four of its metal complexes could inhibit the growth where the inhibition zone diameter follow the order Ni(II) (31 mm) > Cr(III) (26 mm) > Co(II) (17 mm) > parent Schiff base (16 mm) > cefepime standard (12 mm). With respect to *A. niger*, the parent schiff

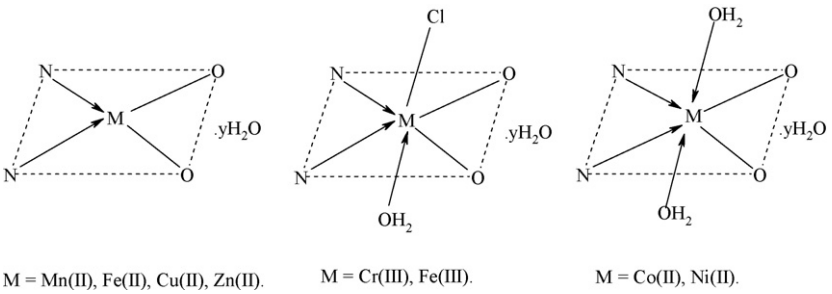

Fig. 4. Proposed structures of metal complexes.

Table 7
Antifungal assay of H_2L and its metal complexes.

Compounds	*Aspergillus flavus*		*Aspergillus niger*	
	Inhibition zone diameter (mm)	Inhibition (%)	Inhibition zone diameter (mm)	Inhibition (%)
Control	0	0	0	0
H_2L	16	17.7	15	16.6
$[CrCl(L)(H_2O)]\cdot H_2O$	26	28.8	24	26.6
$[Mn(L)]\cdot H_2O$	0	0	0	0
[Fe(L)]	0	0	0	0
$[FeCl(L)(H_2O)]\cdot 2H_2O$	0	0	0	0
$[Co(L)(H_2O)_2]$	17	18.8	19	21.1
$[Ni(L)(H_2O)_2]\cdot 2H_2O$	31	34.4	28	31.1
$[Cu(L)]\cdot 2H_2O$	0	0	0	0
[Zn(L)]	0	0	0	0
Cefepime	12	13.3	10	11
L.S.D. 1% 5%	2.471.52		2.251.29	

Table 8
Antibacterial assay of H_2L and its metal complexes.

Compounds	*Escherichia coli*		*Staphylococcus aureus*	
	Inhibition zone diameter (mm)	Inhibition (%)	Inhibition zone diameter (mm)	Inhibition (%)
Control	0	0	0	0
H_2L	0	0	0	0
$[CrCl(L)(H_2O)]\cdot H_2O$	14	15.5	11	12.2
$[Mn(L)]\cdot H_2O$	12	13.3	10	11.1
[Fe(L)]	0	0	0	0
$[FeCl(L)(H_2O)]\cdot 2H_2O$	0	0	0	0
$[Co(L)(H_2O)_2]$	0	0	0	0
$[Ni(L)(H_2O)_2]\cdot 2H_2O$	0	0	0	0
$[Cu(L)]\cdot 2H_2O$	0	0	0	0
[Zn(L)]	0	0	0	0
Cefepime	10	11	8	8.87

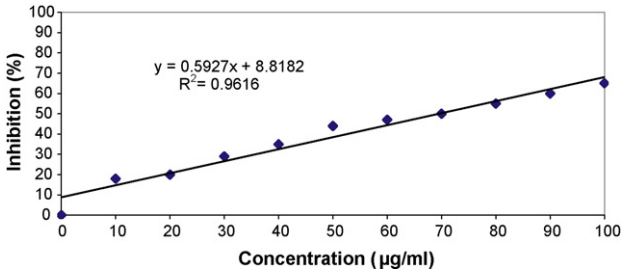

Fig. 5. Determination of MIC of H_2L and its metal complexes on the growth of *Aspergillus flavus* by disk diffusion method.

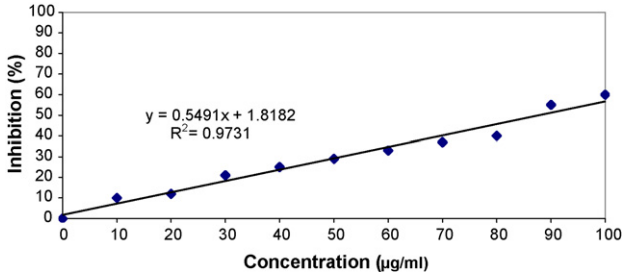

Fig. 6. Determination of MIC of H_2L and its metal complexes on the growth of *Aspergillus niger* by disk diffusion method.

base and four of its metal complexes inhibited the growth. The inhibition was attained in the order Ni(II) > Cr(III) > Co(II) > Schif base > cefepime standard where the inhibition zones were 28, 24, 19, 15 and 10 mm in diameter, respectively.

H_2L and some metal complexes: Fe(II), Fe(III), Cu(II), Co(II) and Zn(II) virtually lack any noticeable antibacterial activities. The antibacterial activity of H_2L ligand and its metal complexes was carried out and the data obtained are shown in Table 8. With regard to *S. aureus* (Gram-positive), the data show that only two metal complexes inhibited the growth where the inhibition zone diameters reached 11 and 10 mm in case of Cr(III) and Mn(II) complexes, respectively. Their biological activities are higher that of cefepime standard (inhibition zone is found to be 8 mm).

With regard to *E. coli* (Gram-negative), the data in Table 8 shows that only two metal complexes together with the cefipime standard inhibited the growth where the inhibition zone diameters reached 14, 12 and 10 mm in case of Cr(III), Mn(II) complexes and cefepime standard, respectively.

Table 9
Antimicrobial activities of the compounds tested as evaluated by the minimum inhibitory concentration (MIC, μg/ml).

Test organism	H_2L	Cr(II)	Mn(II)	Co(II)	Ni(II)
Aspergillus flavus	120	55	0	110	70
Aspergillus niger	150	65	0	140	80
Escherichia coli	0	120	130	0	0
Staphyllococcus aureus	0	100	105	0	0

3.12. Determination of MIC

Regression analysis was carried out for data. The correlation coefficient (r^2) was calculated to measure the strength of the relation between two variables x and y. The equation of the regression line was given. Figs. 5 and 6 show determination of MIC of H_2L and its metal complexes on the growth of *A. flavus* (Fig. 5) and *A. niger* (Fig. 6) by disk diffusion method.

In case of *A. flavus*, Table 9 shows that Cr(III) showed the least MIC (55 μg/ml), followed by Ni(II) (70 μg ml^{-1}), Co(II) (110 μg ml^{-1}) and H_2L (120 μg ml^{-1}). In case of *A. niger*, Table 9 shows that Cr(III)

showed the least MIC (65 μg ml^{-1}), followed by Ni(II) (80 μg ml^{-1}), Co(II) (140 μg ml^{-1}) and H_2L (150 μg ml^{-1}). The complexation with Cr(III) and Ni(II) ions can somewhat increase the activities of H_2L against the tested fungal species.

Non-substituted *o*-aminophenol is known as Questiomycin B antibiotic with specific antifungal (antimycobacterial) activity [29]. Cr(III) complex can employed as an agent to render the microbe non-invasive [30]. In evaluating the antibacterial activity of Cr(III) and Mn(II) complex, we can note that they also demonstrated a low antibacterial activity toward *E. coli* (Gram-negative), the MIC was 120 and 130 μg ml^{-1}, respectively (Table 9). The estimated antibacterial activity results against *S. aureus* (Gram-positive) show that the MIC was 100 and 105 μg ml^{-1}, respectively. Gram-positive bacteria are more sensitive to the tested metal complexes. The complexation with Cr(III) and Mn(II) ions can somewhat increase the activities of H_2L against Gram-positive more than Gram-negative bacteria. It is well known that the bacterial cell wall is a good target for antimicrobial agents, metal complexes among them. In general, we have revealed a significant difference of MIC for the H_2L and its Cr(III) and Mn(II) complex under study against Gram-positive and Gram-negative bacteria. The latter finding is accounted for by the fact that the first barrier capable of limiting antimicrobial activities is the outer membrane of Gram-negative bacteria. This fact is widely known and referred to as 'intrinsic resistance' of Gram-negative bacteria.

Schiff bases are important class of compounds in medicinal and pharmaceutical field. They show biological applications including antibacterial activity [5–7] whereas in some cases, metal complexes are less toxic than the parent drugs [31]. Cr(III), $[Cr(salen)(OH_2)_2]^+$, has an inhibitory action on the growth and invasive and pathogenic potential of *S. Dysenteriae* [30]. Thus, our investigation showed that some metal complexes may be more active than the parent Schiff base and cefepime standard and they may be of interest in designing new drugs. The tested H_2L and its metal complexes showed promising antifungal activity and weak antibacterial activity.

References

[1] Y. Elerman, M. Kabak, A. Elmali, Z. Naturforsch. B 57 (2002) 651.
[2] M.M.H. Khalil, M.M. Abualy, R.M. Ramadan, Spectrochim. Acta (Part) 61 (2005) 157.
[3] N. Chantarasiri, V. Ruangpornvisuti, N. Muangsin, H. Detsen, T. Mananunsap, C. Batiya, N. Chaichit, J. Mol. Struct. 701 (2004) 93.
[4] A.A. Soliman, G.G. Mohamed, J. Thermochim. Acta 421 (2004) 151.
[5] A.A.A. Abu-Hussen, J. Coord. Chem. 59 (2006) 157.
[6] M.S. Karthikeyan, D.J. Parsad, B. Poojary, K.S. Bhat, B.S. Holla, N.S. Kumari, Bioorg. Med. Chem. 14 (2006) 7482–7489.
[7] P. Panneerselvam, R.R. Nair, G. Vijayalakshmi, E.H. Subramanian, S.K. Sridhar, Eur. J. Med. Chem. 40 (2005) 225.
[8] O.M. Walsh, M.J. Meegan, R.M. Prendergast, T.A. Nakib, Eur. J. Med. Chem. 31 (1996) 989.
[9] (a) L.A. Finney, T.V. O'Halloran, Science 300 (2003) 931;
(b) D. Mustafi, A. Bekesi, B.G. Vertessy, M.W. Makinen, Proc. Natl. Acad. Sci. (USA) 100 (2003) 5670.
[10] K.A. Marr, R.A. Carter, F. Crippa, A. Wald, L. Corey, Clin. Infect. Dis. 34 (2002)909.
[11] F. Barchiesi, E. Spreghini, A. Santinelli, A.W. Fothergill, S. Fallani, E. Manso, E. Pisa, D. Giannini, A. Novelli, M.I. Cassetta, T. Mazzei, M.G. Rinaldi, G. Scalise, Antimicrob. Agents Chemother. 49 (2005) 5133.
[12] J. Dotis, E. Roilides, Int. J. Infect. Dis. 8 (2004) 103.
[13] X. Bosch, Lancet 353 (1999) 131.
[14] G.G. Mohamed, Spectrochim. Acta (Part A) 64 (2006) 188.
[15] G.G. Mohamed, M.M. Omar, Ahmed M.M. Hindy, Turkish J. Chem. 30 (2006) 361.
[16] G.G. Mohamed, C.M. Sharaby, Spectrochim. Acta (Part A) 66 (2007) 949.
[17] M.M. Omar, G.G. Mohamed, M.M. Ahmed, J. Hindy, Thermal Anal. Cal. 86 (2006) 315.
[18] D.H. Lorone, Medically important fungi. A guide to identification, 3rd ed., ASM Press, Washington, D.C., 1995.
[19] S. Arikan, P.M. Lozano-Chiu, J.H. Rex, Agents Chemother. 45 (2002) 327.
[20] National Committee for Clinical Laboratory Standards. Performance standard for antimicrobial disk susceptibility testing. NCCLS publication no. M2-A6. National Committee for Clinical Laboratory Standards, Wayne, Pa. (1997).
[21] G.N. Pershin (Ed.), Methods of the Experimental Chemotherapy, Meditsina, Moskwa, 1971, p. 103.
[22] M.M. Omar, G.G. Mohamed, Spectrochim. Acta (Part A) 61 (2005) 929.
[23] F.A. Cotton, G. Wilkinson, C.A. Murillo, M. Bochmann, Advanced Inorganic Chemistry, Sixth ed., Wiley, New York, 1999.
[24] M.M. Moustafa, J. Thermal Anal. Cal. 50 (1997) 463.
[25] M.F.R. Fouda, M.M. Abd-el-Zaher, M.M.E. Shadofa, F.A. El Saied, M.I. Ayad, A.S. El Tabl, Trans. Met. Chem. 33 (2008) 219.
[26] S. Chandra, U. Kuar, Spectrochim. Acta (Part A) 61 (2005) 219.
[27] K.B. Gudasi, S.A. Patil, R.S. Vadavi, R.V. Shenoy, Trans. Met. Chem. 31 (2006) 586.
[28] A.W. Coats, J.P. Redfern, Nature 20 (1964) 68.
[29] K. Anzai, K. Isono, K. Okuma, S. Suzuki, J. Antibiot. (Ser. A) 13 (1960) 125.
[30] H.Y. Shrivastava, S.N. Devaraj, B.U. Nair, J. Inorg. Biochem. 98 (2004) 387.
[31] S.J. Lippard, J.M. Berg (Eds.), Principles of Bioinorganic Chemistry, University Science Books, Mill Valley, CA, 1994.